Synchronized charge oscillations in correlated electron systems

Nikhil Shukla[1], Abhinav Parihar[2], Eugene Freeman[1], Hanjong Paik[3], Greg Stone[4], Vijaykrishnan Narayanan[5], Haidan Wen[6], Zhonghou Cai[6], Venkatraman Gopalan[4], Roman Engel-Herbert[4], Darrell G. Schlom[3,7], Arijit Raychowdhury[2] & Suman Datta[1*]

S1. Characterization of E_2 / E_1 and oscillator stability

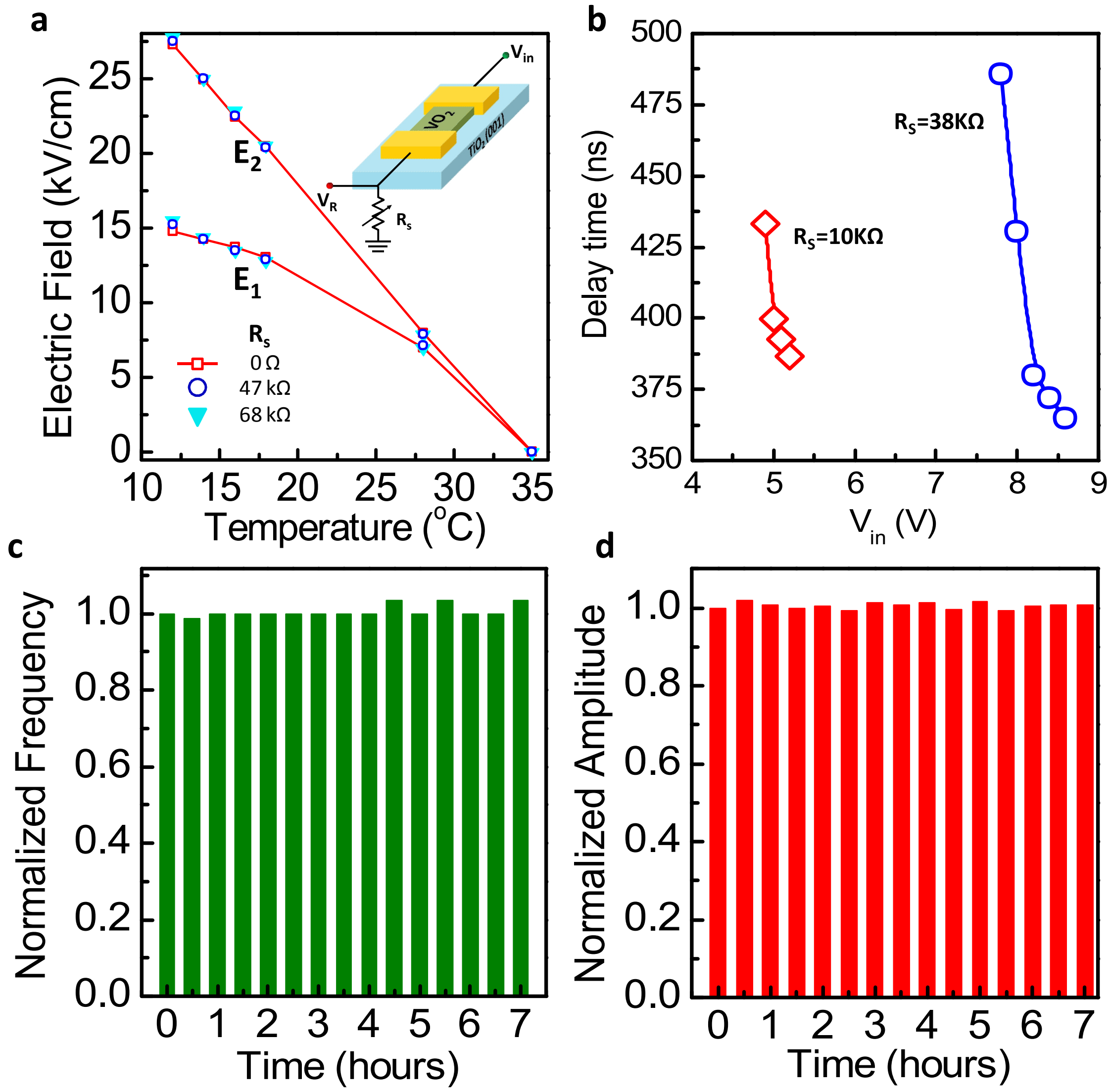

Figure S1 | Characterization of critical field E_2 / E_1 and oscillator stability (a) Variation of critical electric field E_2 and E_1 as a function of temperature for different values of series resistance R_s (=0Ω, 47kΩ, 68kΩ). Inset show the circuit schematic for this measurement. The electric field across the VO_2 device is calculated as $(V_{in}-V_R)/L_{VO2}$. R_s does not affect the threshold points E_2 and E_1 associated with the electrically driven phase transition. E_2 associated with the IMT is more sensitive to temperature than E_1 which is associated with the MIT. (b) The delay time for the VO_2 films used in the oscillators. The delay times are specified for the bias range in which oscillations are realized (region of interest) and do not vary much with R_S. The offset in V_{in} is due to different values of R_S. (c) Temporal variation of oscillation frequency (d) Oscillation amplitude with respect to t=0 hours over an extended period of time (t=7hours). The frequency and amplitude remain relatively stable over > 2.5 $x10^9$ cycles. f(0)=115.999kHz; A(0)=2.914V. The measurements were sampled every 0.5hr.

E_2 and E_1 are the critical electric fields associated with the electrically driven insulator-to-metal transition (IMT) and metal-to-insulator transition (MIT) in VO_2, respectively. As described in the main text, irrespective of the physical origin of the phase transition, these fields (at a fixed temperature) enable us to control the state (metallic/insulating) of the VO_2 during the electrically driven the phase transition. Fig. 1a shows the variation of E_2 and E_1 as a function of temperature for different values of series resistance R_s including R_s=0 Ω. It is clear that E_2 and E_1 increase at lower temperature as we move further away from the transition temperature (T_c=35°C) and that E_2 is more sensitive to temperature than E_1. Further, R_s, and the negative feedback that it provides do not affect the value of E_2 and E_1. Knowing the magnitude of these critical fields enables us to design the dynamics of the VO_2 relaxation oscillators.

The delay time[22] for the VO_2 films (for R_S=10kΩ, 38kΩ) as a function of the trigger DC voltage is shown in Fig. 1b (the delay times are specified for the bias range in which oscillations are realized). This suggests that metal-insulator transition may be controlled by the electric field wherein the underlying mechanism for the transition is field induced nucleation[22].

Figure 1(c,d) shows the variation of frequency and amplitude of oscillation in VO_2 oscillators over an extended period of time (7 hours; > 2.5 x10^9 oscillation cycles). The measurements were sampled every 0.5hr. It is clear that frequency and amplitude of oscillations remains stable over this period of time. The maximum deviation in frequency and amplitude with respect to t=0 hours is 3.44% and 1.93%, when measured over 7 hours of continuous operation. Additionally, when two such oscillators are coupled, the frequency and amplitude of the coupled are expected to stabilize further due to the mutual feedback that each oscillator provides to the other.

S2. Modelling negative feedback provided by R_s

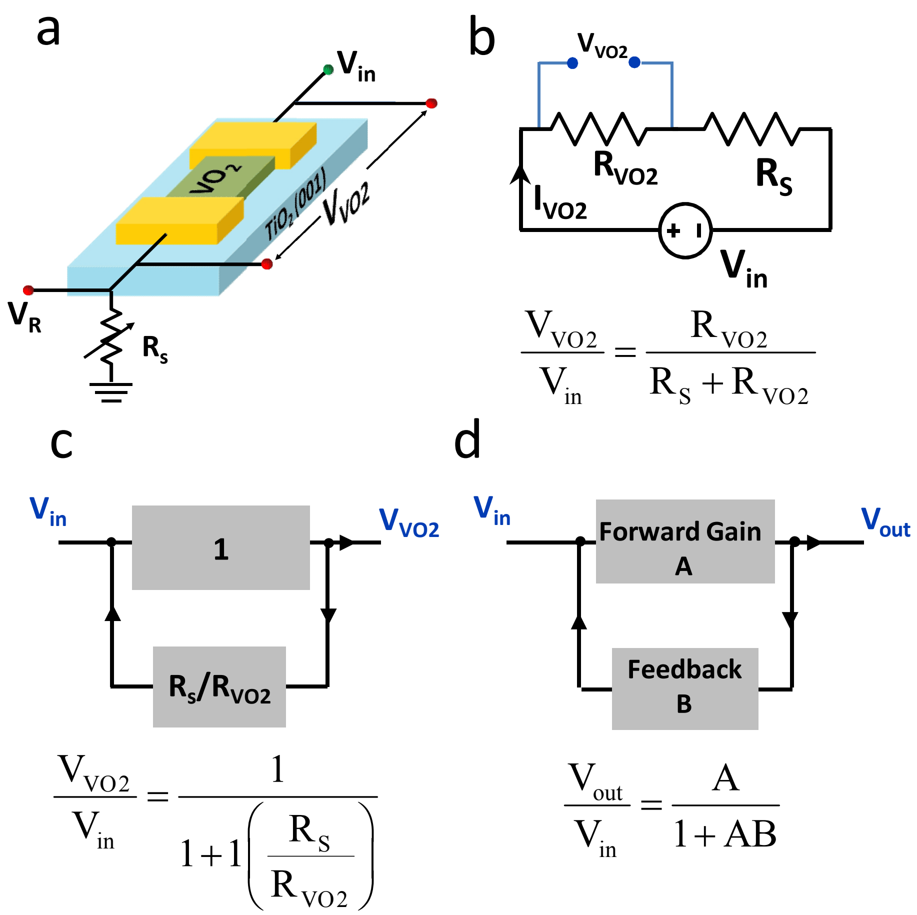

Figure S2 | Negative feedback provided by R_s (a) Schematic of the VO_2 circuit that exploits negative feedback from the series resistor, R_s, to induce a non-hysteretic phase transition. (b) Electrical equivalent circuit of the schematic in (a). (c) The VO_2 circuit represented as an equivalent control system with feedback. The equation in the diagram is the transfer function for the system (d) General representation of the control system with feedback. Comparing (c) and (d) the forward gain A=1; feedback factor $B=R_s/R_{VO2}$ which provides negative feedback induced by R_s. The equation in the diagram is the transfer function for the system.

Figure S2a shows the schematic of a VO_2 circuit that uses negative feedback from the series resistor R_s to induce a non-hysteretic transition.

Applying Kirchhoff's voltage law to the electrical equivalent circuit shown in Fig. S2b

$$\frac{V_{VO2}}{V_{in}} = \frac{R_{VO2}}{R_S + R_{VO2}} \tag{S2.1}$$

$$\frac{V_{VO2}}{V_{in}} = \frac{1}{1+1\frac{R_s}{R_{VO2}}} \tag{S2.2}$$

$$\frac{V_{out}}{V_{in}} = \frac{A}{1+AB} \tag{S2.3}$$

The equivalent representation of the circuit along with the standard representation a control system with feedback is shown in Fig. S2(c,d). Comparing equation (S2.2) with equation (S2.3) which is the standard expression for a control system with a forward loop gain A and feedback B, the forward loop gain and feedback for VO_2 circuit is given as

$$A = 1; B = \frac{R_s}{R_{VO2}} \tag{S2.4}$$

where $B = \frac{R_s}{R_{VO2}}$ is the negative feedback term generated due to R_s.

S3. Modulation of current-electric field characteristics using R_s

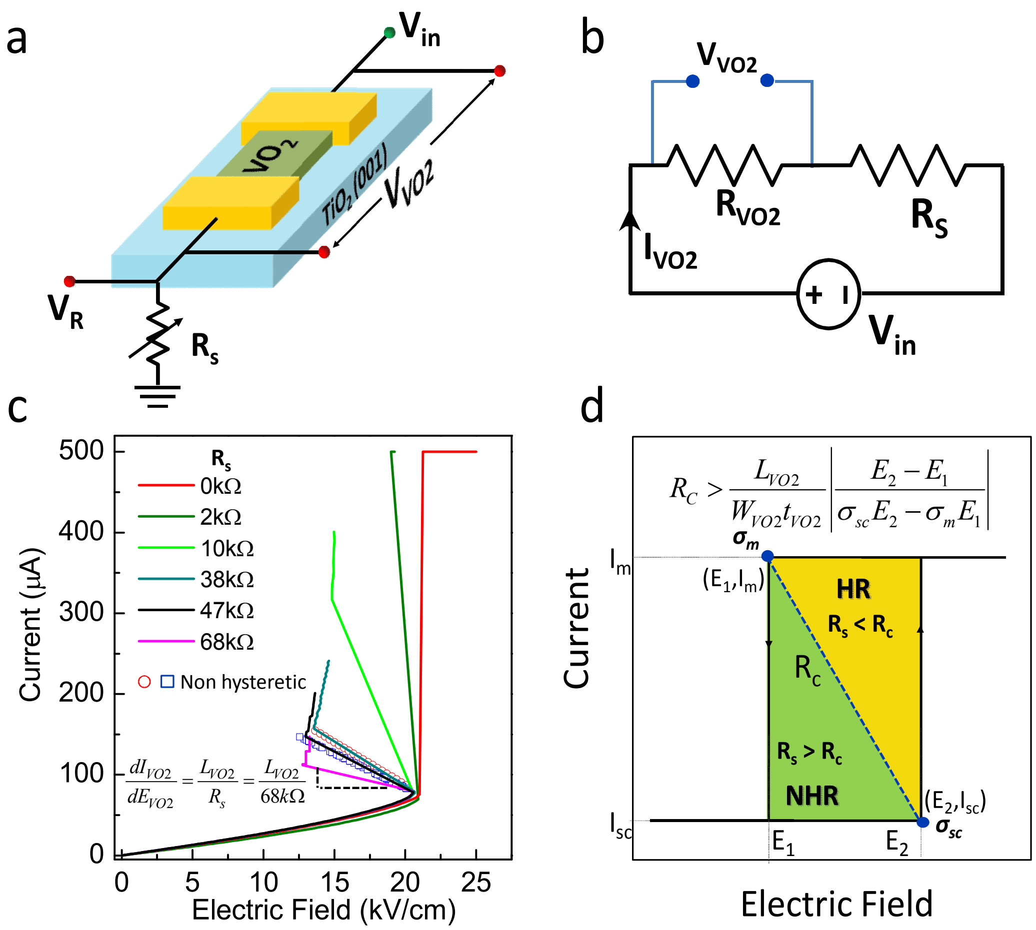

Figure S3 | Modulating VO_2 phase transition dynamics using R_s (a) Schematic of the circuit used to access and stabilize the non-hysteretic transition regime in VO_2. (b) Electrical equivalent circuit of the schematic shown in (a). Since we consider only the DC current-electric field characteristics here, VO_2 in the unstable phase transition regime is treated only as a variable resistor (R_{VO2}). (c) The series resistance R_s modifies the dynamics of the electrically induced phase transition in VO_2 through a process of negative feedback such that the slope of the current-electric field characteristics in the vicinity of the phase transition equals $-R_s/L_{VO2}$; $dI_{VO2}/dE_{VO2} = -R_s/L_{VO2}$ (or $dI_{VO2}/dV_{VO2} = -R_s$). This allows access to a regime where a non-hysteretic reversible transition may be obtained. It must be noted that a non-hysteretic transition (shown for R_s=38 kΩ (red circle), =47kΩ (blue square)) can be achieved only if no additional electric field is used to drive the system further into the metallic state. Otherwise a hysteresis will be introduced (solid lines). (d) Schematic illustration of the critical series resistance R_c that sets the criteria for stabilization of non-hysteretic regime. σ_m and σ_m are the equivalent conductivities in the metallic and insulating states respectively.

Figure S3a shows the schematic of a VO_2 circuit that uses negative feedback from a series resistor R_s to induce a non-hysteretic transition.

For the circuit shown in Fig. S3b, VO_2 behaves as a variable resistor across the phase transition. Appling Kirchhoff's voltage law to the circuit in Fig. S3b we find

$$V_{VO2} = \frac{V_{in} R_{VO2}}{R_{VO2} + R_S} \qquad \text{(S3.1)}$$

and

$$I_{VO2} = \frac{V_{in}}{R_{VO2} + R_S} \qquad \text{(S3.2)}$$

Differentiating equation (S3.1) and equation (S3.2) with respect to R_{VO2}

$$\frac{dV_{VO2}}{dR_{VO2}} = \frac{V_{in} R_S}{(R_{VO2} + R_S)^2} \qquad \text{(S3.3)}$$

and

$$\frac{dI_{VO2}}{dR_{VO2}} = -\frac{V_{in}}{(R_{VO2} + R_S)^2} \qquad \text{(S3.4)}$$

Combining equation (S3.3) and equation (S3.4) leads to

$$\frac{dV_{VO2}}{dI_{VO2}} = \left(\frac{dV_{VO2}}{dR_{VO2}}\right) / \left(\frac{dI_{VO2}}{dR_{VO2}}\right) = -R_S \qquad \text{(S3.5)}$$

$$L_{VO2} \frac{dE_{VO2}}{dI_{VO2}} = -R_S \qquad \text{(S3.6)}$$

From equation (S3.5) and equation (S3.6) it is clear that the slope of the negative differential resistance (NDR) region is exactly equal to the external series resistance (R_s) (normalized to the VO_2 channel length in the case of electric field). Further, integrating equation (S3.6) describes the current-electric field characteristic across VO_2

$$V_{VO2} = C - I_{VO2} R_S \qquad \text{(S3.7)}$$

where C is the constant of integration

Expressing equation (S3.7) in terms of electric field

$$E_{VO2} = C_1 - \Delta I_{VO2} R_S / L_{VO2} \qquad \text{(S3.8)}$$

where constant of integration C_1=E_2 and $\Delta I_{VO2} = I_{VO2}(E_{VO2}) - I_{VO2}(E_2)$ and L_{VO2} is the length of the VO_2 channel. Substituting the integration constant, equation (S3.8) is expressed as

$$E_{VO2} = E_2 - \Delta I_{VO2} R_S / L_{VO2} \tag{S3.9}$$

Therefore using R_s, the current-electric field characteristics (equation (S3.9)) can be modified as shown in Fig. S3c such that the electric field across the VO_2 drops to below E_1 as it undergoes the IMT. This causes the metallic phase to be unstable and if no additional electric field is used to drive it further into the metallic state, the VO_2 channel will spontaneously return to the insulating state leading to a non-hysteretic and reversible phase transition (red circles, blue squares in Fig. S3c). It should be noted that even with an appropriate series resistor R_s ($>R_c$), if the VO_2 device is driven further into the metallic state (using an electric field) as it completes the IMT, an hysteresis will be introduced (solid lines in Fig. S3c).

The calculation of the critical resistance R_c that can enable a non-hysteretic transition is shown in Fig. S3d. The fundamental criterion for the non-hysteretic transition is that the electric field across VO_2 should drop to E_1 (or below) before the VO_2 completes the IMT and becomes completely metallic.

The critical negative differential conductance dI_{VO2}/dE_{VO2} (expressed in terms of electric field) for a non-hysteretic transition is illustrated in Fig. S3d and is given as

$$\frac{dI_{VO2}}{dE_{VO2}} = \frac{I_m - I_{sc}}{E_2 - E_1} = W_{VO2} t_{VO2} \frac{\sigma_m E_1 - \sigma_{sc} E_2}{E_1 - E_2} \tag{S3.10}$$

Equating equation (S3.10) and equation (S3.6) and rearranging we get

$$\frac{1}{R_c} = \frac{W_{VO2} t_{VO2}}{L_{VO2}} \left| \frac{\sigma_m E_1 - \sigma_{sc} E_2}{E_1 - E_2} \right| \tag{S3.11}$$

$$R_C > \frac{L_{VO2}}{W_{VO2} t_{VO2}} \left| \frac{E_2 - E_1}{\sigma_{sc} E_2 - \sigma_m E_1} \right| \tag{S3.12}$$

S4. In-situ Nano-X-Ray Diffraction of VO_2 film stabilized in an oscillating state

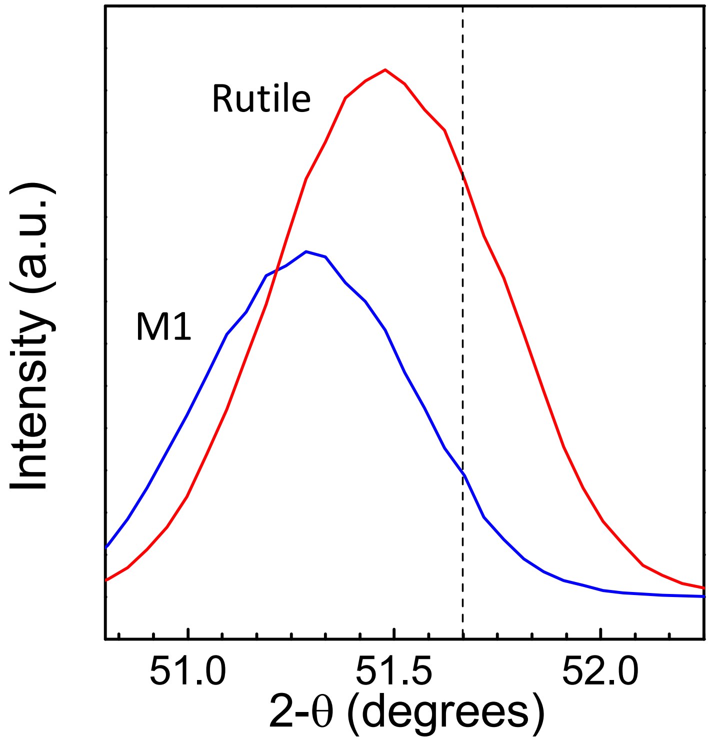

Figure 4 | Bragg peaks for nano X-ray diffraction measurement $[40\bar{2}]$ and $[002]$ Bragg peaks of the M1 and rutile phase of VO_2, respectively. The dashed line indicates the θ/2θ angle at which the XRD measurement was performed. This figure is the same as the inset in Fig.1e of the main text.

In-situ nano-X-ray diffraction study of the VO_2 film stabilized in an oscillating state in the NDR regime is performed to confirm the nature of the structural phases involved in the transition. The experiments are performed at ID2-D beam line at the Advanced Photon source, Argonne National labs, USA.

The experimental setup (ref [43] for details of the nano X-ray set up) consists of a DC source to apply input bias, a digital oscilloscope to read out electrical oscillation output, a delay generator to sample the oscillator waveform and synchronize the photon counter to the rising edge of the oscillator output. The delay generator is programmed to produce four 20 μs square pulses with 40 μs periods creating 20 μs time windows starting at 0, 40, 80, and 120μs with respect to the rising edge labelled as t_1-t_4 respectively. The X-ray diffraction intensity for the four different time windows was measured by a single photon detector and integrated over 200 seconds.

Figure 4 shows the $[002]$ Bragg peaks of the M1 and rutile phase of VO_2 respectively and Structural phase information is resolved using contrast in the number of photon counts. This is achieved by positioning the detector at a fixed 2θ angle (=51.714^o) to achieve high contrast between the R $[002]$ and M1$[40\bar{2}]$. This experimental setup produces a high photon (diffraction) count for the rutile phase relative to the monoclinic M1 phase.

S5. Coupled oscillator simulation macro-model

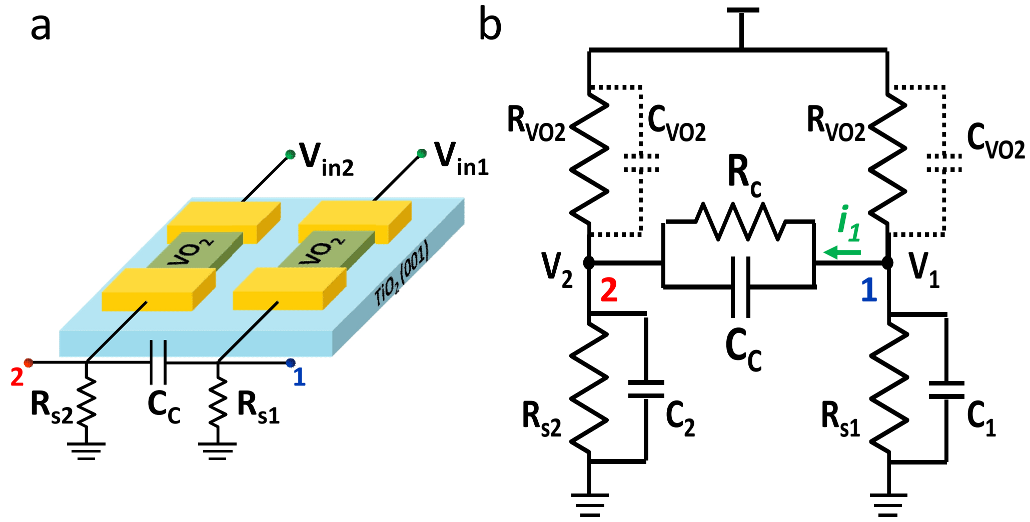

FigureS5 | Equivalent circuit for coupled oscillator macro-model (a) Schematic of the capacitively coupled oscillator circuit. (b) Macro-model of the coupled system of VO_2 relaxation oscillators used to simulate the frequency locking behavior. C_1 and C_2 are the effective capacitance of each oscillator, which includes the VO_2 capacitance associated with the VO_2 film and the device (C_{VO2}) as well as parasitic capacitance. The coupling capacitor is assumed to be non-leaky ($R_c \rightarrow \infty$). i_1 is the ac current flowing through the coupling capacitor C_C

Figure S5a shows the schematic of the capacitively coupled VO_2 oscillator circuit. The VO_2 device can be represented using its DC resistances for both the metallic and the insulating states. The domain capacitance C_{VO2} and the parasitic capacitance in each oscillator circuit are represented by an equivalent capacitance. This can be used to model and analyze the proposed relaxation oscillator as illustrated in the compact model in Fig. S5b. Applying Kirchhoff's current law at the node 1 of oscillator 1, we can write

$$C_1 \frac{dV_1}{dt} = \frac{V - V_1}{R_{VO2}} - \frac{V_1}{R_{S1}} - i_1 \qquad \text{(S5.1)}$$

where C_1 includes contributions from the device (domain capacitance C_{VO2}) as well as parasitic capacitances, R_{S1} is the series resistance and R_{VO2} is the VO_2 device resistance. Alternatively we can write this as

$$C_1 \frac{dV_1}{dt} = \frac{V_{in}}{R_{VO2}} - \left(\frac{V_1}{R_{VO2}} + \frac{V_1}{R_{S1}} \right) - i_1 \qquad \text{(S5.2)}$$

where V_{in} is the input voltage to oscillator. In the process of charging C_1, VO_2 is in the metallic state and $R_{VO2}=R_M$ ($<<R_{S1}$) where R_M is the resistance of the VO_2 device in the metallic state. Equation (S5.2) then reduces to

$$C_1\frac{dV_1}{dt}=\frac{V_{in}}{R_M}-\frac{V_1}{R_M}-i_1 \tag{S5.3}$$

Similarly, when C_1 is discharging, the VO_2 is in an insulating state and $R_{VO2}=R_I$ ($>>R_{S1}$) where R_I is the resistance of the VO_2 device in the insulating state. Equation (S5.2) reduces to

$$C_1\frac{dV_1}{dt}=\frac{V_{in}}{R_I}-\frac{V_1}{R_{S1}}-i_1 \tag{S5.4}$$

The current, responsible for the coupling can be expressed as

$$i_1=\frac{V_1-V_2}{R_C}+C_C\frac{d(V_1-V_2)}{dt} \tag{S5.5}$$

where C_C is the coupling capacitor and R_C (typically very high and in the order of GΩ) represents any leakage current through the capacitor. This leads to a generic form for equation (S5.2) for the coupled node 1 and 2 and can be expressed as a set of ordinary differential equations (ODEs)

$$C_1V_1^{'}=\frac{V_{in}}{R_{VO2}}-\left(\frac{V_1}{R_{VO2}}+\frac{V_1}{R_{S1}}\right)-\frac{V_1-V_2}{R_C}-C_C\left(V_1^{'}-V_2^{'}\right) \tag{S5.6a}$$

and

$$C_2V_2^{'}=\frac{V_{in}}{R_{VO2}}-\left(\frac{V_2}{R_{VO2}}+\frac{V_2}{R_{S2}}\right)-\frac{V_2-V_1}{R_C}-C_C\left(V_2^{'}-V_1^{'}\right) \tag{S5.6b}$$

where $V_1^{'}$ and $V_2^{'}$ are the time derivatives of V_1 and V_2 respectively. The correct approximations as shown in equation (S5.3) and equation (S5.4) have to be evoked for the charging and the discharging regimes. Simplifying equation (S5.6), we arrive at the following set of ODEs that represent the dynamics of the coupled oscillator system

$$V_1^{'}=\frac{C_C+C_2}{C_{eff}}\left(\frac{V_{in}}{R_{VO2}}-\left(\frac{V_1}{R_{VO2}}+\frac{V_1}{R_{S1}}\right)\right)+\frac{C_C}{C_{eff}}\left(\frac{V_{in}}{R_{VO2}}-\left(\frac{V_2}{R_{VO2}}+\frac{V_2}{R_{S2}}\right)\right)+\frac{C_2}{C_{eff}}\frac{V_1-V_2}{R_C} \tag{S5.7a}$$

and

$$V_2' = \frac{C_C + C_1}{C_{eff}}\left(\frac{V_{in}}{R_{VO2}} - \left(\frac{V_2}{R_{VO2}} + \frac{V_2}{R_{S2}}\right)\right) + \frac{C_C}{C_{eff}}\left(\frac{V_{in}}{R_{VO2}} - \left(\frac{V_1}{R_{VO2}} + \frac{V_1}{R_{S1}}\right)\right) + \frac{C_2}{C_{eff}}\frac{V_2 - V_1}{R_C} \qquad \text{(S5.7b)}$$

where

$$C_{eff} = C_C C_1 + C_C C_2 + C_1 C_2$$

Equation (S5.7) is numerically solved by considering the correct operating regime VO_2 device and this enables us to capture the dynamics of the coupled oscillator system.

References

43. Soh, Y.-A. *et al.* Local mapping of strain at grain boundaries in colossal magnetoresistive films using x-ray microdiffraction. *J. Appl. Phys.* **91,** 7742 (2002).